ELSEVIER

Biophysical Chemistry 121 (2006) 209 – 217

Biophysical Chemistry

http://www.elsevier.com/locate/biophyschem

Direct electron transfer between hemoglobin and pyrolytic graphite electrodes enhanced by Fe_3O_4 nanoparticles in their layer-by-layer self-assembly films

Dongfang Cao, Naifei Hu *

Department of Chemistry, Beijing Normal University, Beijing 100875, China

Received 19 September 2005; received in revised form 5 November 2005; accepted 6 November 2005
Available online 21 Febuary 2006

Abstract

Alternate adsorption of negatively charged Fe_3O_4 nanoparticles from their pH 8.0 aqueous dispersions and positively charged hemoglobin (Hb) from its pH 5.5 buffers on solid substrates resulted in the assembly of $\{Fe_3O_4/Hb\}_n$ layer-by-layer films. Quartz crystal microbalance (QCM), UV–vis spectroscopy, and cyclic voltammetry (CV) were used to monitor and confirm the film growth. A pair of well-defined, nearly reversible CV peaks for HbFe(III)/Fe(II) redox couples was observed for $\{Fe_3O_4/Hb\}_n$ films on pyrolytic graphite (PG) electrodes. Although the multilayered films grew linearly with the number of Fe_3O_4/Hb bilayers (n) and the amount of Hb adsorbed in each bilayer was generally the same, the electroactive Hb could only extend to 6 bilayers. This indicates that only those Hb molecules in the first few bilayers closest to the electrode surface are electroactive. The electrochemical parameters such as the apparent heterogeneous electron transfer rate constant (k_s) were estimated by square wave voltammetry (SWV) and nonlinear regression. The Soret absorption band position of Hb in $\{Fe_3O_4/Hb\}_6$ films showed that Hb in the films retained its near native structure in the medium pH range. The $\{Fe_3O_4/Hb\}_6$ film electrodes also showed good biocatalytic activity toward reduction of oxygen, hydrogen peroxide, trichloroacetic acid, and nitrite. The electrochemical reduction overpotentials of these substrates were lowered significantly by $\{Fe_3O_4/Hb\}_n$ films.

Keywords: Hemoglobin; Fe_3O_4 nanoparticle; Layer-by-layer assembly; Direct electrochemistry; Electrocatalysis

1. Introduction

The direct electrochemistry of redox proteins can be achieved by immobilizing the proteins into appropriate films on electrode surface [1,2]. The study on direct electron transfer of proteins can be employed as a model in the mechanistic study of electron exchange among enzymes in biological systems, and serve as a foundation for fabricating electrochemical biosensors and bioreactors without using chemical mediators [3,4]. Recently, the layer-by-layer self-assembly [5] has opened up a new approach to immobilize and organize proteins into ultrathin films according to a predesigned architecture [6,7]. These protein layer-by-layer films were usually fabricated by alternate adsorption of oppositely charged proteins and polyelectrolytes from their solution. The stable protein films constructed by this method have been successfully applied to the study of direct electrochemistry of redox proteins or enzymes at electrodes [8–12]. The layer-by-layer assembly demonstrates obvious advantages over cast and dipping methods in its precise control of film composition and thickness on the nanometer scale, and over self-assembled monolayer (SAM) and Langmuir–Blodgett (LB) membrane methods in its flexibility and simplicity, and thus is more suitable to the study of direct electrochemistry of proteins.

The layer-by-layer assembly has also been extended to construct protein films with nanoparticles. For example, Kunitake et al. achieved spatially controlled films of cytochrome c (Cyt c) with TiO_2 nanoparticles by the stepwise deposition/adsorption procedure [13]. Willner et al. assembled multilayered microperoxidase-11/Au-nanoparticle films that acted as electrochemical catalysts for reduction of H_2O_2 [14]. Lvov and coworkers made Mb films assembled layer-by-layer with MnO_2 or SiO_2 nanoparticles [15]. Recently, we reported heme protein

* Corresponding author. Tel.: +86 10 58805498; fax: +86 10 58802075.
E-mail address: hunaifei@bnu.edu.cn (N. Hu).

0301-4622/$ - see front matter © 2005 Elsevier B.V. All rights reserved.
doi:10.1016/j.bpc.2005.11.003

films assembled layer-by-layer with clay [16,17], SiO_2 [18,19], and $CaCO_3$ [20] nanoparticles. Inorganic nanoparticles, with their structural stability and small size, provided a favorable microenvironment for redox proteins to transfer electrons with underlying electrodes, and the electrochemical catalysis of various substrates in these films at electrodes were achieved.

The magnetic nanoparticles have attracted an increasing interest with the development of nanostructured materials and nanotechnology in biotechnology and medicine. [21,22]. Among them, Fe_3O_4 nanoparticles are the most commonly used magnetic materials because of their good biocompatibility, strong superparamagnetic property, low toxicity and easy preparation [23–25]. Fe_3O_4 nanoparticles were also used to immobilize enzymes [26,27]. For example, Chen et al. [26] studied the covalent binding of yeast alcohol dehydrogenase (YADH) to Fe_3O_4 nanoparticles via carbodiimide activation. The bound YADH retained most of its original activity and exhibited a 10-fold improved stability compared with the free enzyme. We prepared protein-Fe_3O_4 films by casting the mixture of heme protein solution and Fe_3O_4 nanoparticle dispersion onto pyrolytic graphite (PG) electrodes [28]. Direct electrochemistry and electrocatalysis of the cast protein-Fe_3O_4 films were studied.

The layer-by-layer films containing Fe_3O_4 nanoparticles have also been reported. For instance, the polycations of diazoresin (DR) and negatively charged Fe_3O_4 nanoparticles were assembled into layer-by-layer films on different substrates [29]. The magnetic multilayer films comprised of cationic polydiallyldimethylammonium (PDDA)-coated Fe_3O_4 nanoparticles and anionic polyimides were fabricated on single crystal silicon and quartz substrates by layer-by-layer self-assembly [30]. Kotov and co-workers made free-standing layer-by-layer assembled films composed of alternation layers of Fe_3O_4 nanoparticles and PDDA on cellulose acetate, which was subsequently dissolved in acetone [31].

In the present work, hemoglobin (Hb) and Fe_3O_4 nanoparticles were adsorbed alternately on various solid substrates, and assembled successfully into $\{Fe_3O_4/Hb\}_n$ layer-by-layer films. According to our previous work on cast protein-Fe_3O_4 films [28], we expected that in $\{Fe_3O_4/Hb\}_n$ layer-by-layer films, biocompatible Fe_3O_4 nanoparticles would also provide a favorable microenvironment for Hb to directly exchange electrons with electrodes but with a more precise control of film composition and thickness. To our best knowledge, no report has been published until now on fabricating layer-by-layer films of proteins and Fe_3O_4 nanoparticles. The films were characterized by various techniques, especially by electrochemistry. Electrocatalytic reduction of some substrates of biological or environmental importance was also realized at $\{Fe_3O_4/Hb\}_n$ film electrodes.

2. Experimental

2.1. Chemicals

Bovine hemoglobin (Hb, MW 66,000) and bovine liver catalase (Cat, MW 240,000) were from Sigma and used as received. Fe_3O_4 nanoparticles (diameter ~15 nm) were from Anhui Maanshan Powder Project Co. Poly(ethyleneimine) (PEI, 90%, average MW 60,000) and 3-mercapto-1-propanesulfonate (MPS, 90%) were from Aldrich. Trichloroacetic acid (TCA) was from Beijing Dongjiao Chemical Engineering Plant. Sodium nitrite ($NaNO_2$) was from Beijing Shuanghuan Chemicals. Hydrogen peroxide (H_2O_2, 30%) was from Beijing Chemical Engineering Plant. All other chemicals were reagent grade. Buffers were 0.1 M sodium acetate, 0.05 M sodium dihydrogen phosphate, 0.05 M boric acid, or 0.05 M citric acid, all containing 0.1 M KBr. Buffer pH was adjusted with HCl or KOH. Water was purified twice successively by ion exchange and distillation.

2.2. Film assembly

The aqueous dispersion of Fe_3O_4 nanoparticle (1 mg mL^{-1}) was prepared by ultrasonication for about 2 h in pH 8.0 buffers. The dispersion was ultrasonicated for another 15 min just before the film assembly. TEM results in our previous work [28] showed that the size of Fe_3O_4 nanoparticles in their aqueous dispersions was in the range of 50–80 nm with the average of 65 nm, which was larger than the original size of 15 nm provided by the manufacturer. This indicates that in their aqueous dispersions, Fe_3O_4 nanoparticles aggregate into larger particles, but they are still in the nanometer scale.

For electrochemical studies, basal plane pyrolytic graphite (PG, Advanced Ceramics, geometric area 0.16 cm^2) electrodes were abraded by hand with metallographic sandpaper of 400 grits while flushing with water. Electrodes were ultrasonicated in water for 30 s and dried in air. A precursor layer of positively charged PEI was adsorbed by immersing the PG electrodes into PEI solutions (3 mg mL^{-1}) for 20 min. After being washed with water, the PG/PEI electrodes were alternately immersed for 20 min in an aqueous dispersion of Fe_3O_4 nanoparticles (1 mg mL^{-1}, pH 8.0) and an Hb solution (1 mg mL^{-1}, pH 5.5) with intermediate water washing. This cycle was repeated to obtain the layer-by-layer $\{Fe_3O_4/Hb\}_n$ films with the desirable number of bilayers (n).

For quartz crystal microbalance (QCM) studies, gold-coated resonator electrodes (geometric area 0.196 cm^2) were soaked in freshly prepared piranha solution (3 : 7 volume ratio of 30% H_2O_2 and 98% H_2SO_4) for 10 min at ~95 °C and then washed in pure ethanol and water successively (Caution: the piranha solution is highly corrosive and should be handled with extreme care). The cleaned gold QCM electrodes were immersed in MPS ethanol solutions (4 mM) for 24 h to chemisorb an MPS monolayer on the gold, introducing negative charges on the surface. The following procedure of assembling PEI/$\{Fe_3O_4/Hb\}_n$ films on the Au/MPS surface was the same as on PG electrodes. After each adsorption step, the resonator was washed with water, dried under nitrogen stream, and the frequency was measured in air.

For UV–vis spectroscopic studies, quartz slides were immersed in piranha solution for 5 min, and then carefully rinsed with water and dried with N_2 stream. The procedure of making PEI/$\{Fe_3O_4/Hb\}_n$ films was the same as on PG electrodes.

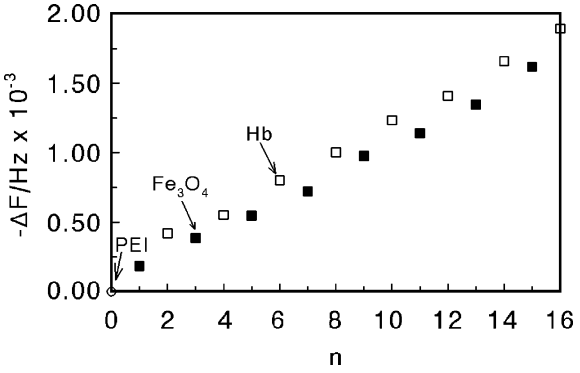

Fig. 1. Shift of QCM frequency with adsorption step for $\{Fe_3O_4/Hb\}_n$ films on Au/MPS/PEI surface: (○) PEI adsorption step, (□) Hb adsorption step, and (■) Fe_3O_4 adsorption step.

2.3. Apparatus and procedures

A CHI 660 electrochemical workstation (CH Instruments) was used for cyclic and square wave voltammetry. A regular three-electrode cell was used with a saturated calomel electrode (SCE) as the reference, a platinum wire as the counter electrode, and a PG disk with films as the working electrode. Voltammetric experiments at film electrodes were performed in buffers containing no proteins. Buffers were purged with highly purified nitrogen for at least 10 min prior to a series of experiments. A nitrogen atmosphere was then maintained during the whole experiment. In the experiments with oxygen, measured volumes of air were injected through solutions via a syringe in a sealed cell, which had been previously deoxygenated with purified nitrogen for 10 min. A CHI 420 electrochemical analyze (CH Instruments) was used for QCM. AT-cut quartz resonators coated by gold thin films on both sides with a fundamental frequency of 8 MHz were used. UV–Vis spectroscopy was done with a Cintra 10e UV–visible spectrophotometer (GBC). All experiments were performed at ambient temperature of 18±2 °C.

3. Results and discussion

3.1. Assembly of $\{Fe_3O_4/Hb\}_n$ layer-by-layer films

With the isoelectric point at 5.9 [32], Fe_3O_4 nanoparticles have negative surface charges at pH 8.0, while Hb has net positive surface charges at pH 5.5 with its isoelectric point at 7.4 [33]. Thus, the main driving force for the assembly of $\{Fe_3O_4/Hb\}_n$ layer-by-layer films is electrostatic interaction between oppositely charged Fe_3O_4 and Hb. After a series of optimization experiments, the most suitable condition, such as pH and concentration of adsorbate solution or dispersion, was selected to assemble the films (see Experimental section), and various techniques were used to monitor or confirm the assembly process.

QCM can detect tiny mass changes on the quartz crystal resonator according to Sauerbrey equation [34]. The relationship between the mass change (g), Δm, and the frequency shift (Hz), Δf, was obtained by taking into account the character of the quartz resonator used in this work:

$$\Delta f = \left(-1.45 \times 10^{8}\right)\Delta m/A \quad (1)$$

where A was the geometric area of the QCM electrode (0.196 cm^2). Thus, 1 Hz frequency decrease corresponded to 1.35 ng mass increase. The QCM data could also be used to estimate the nominal thickness of adsorption layer if assuming that the layer was packed uniformly and densely [6]. The relationship between the nominal thickness (cm), d, and Δf could thus be expressed by

$$d = \left(-3.4 \times 10^{-9}\right)\Delta f/\rho \quad (2)$$

where ρ is the density of the layer material (g cm^{-3}).

When QCM was used to monitor the assembly of $\{Fe_3O_4/Hb\}_n$ films, a roughly linear frequency decrease with adsorption step was observed (Fig. 1), indicating that the growth of the films is uniform and reproducible, and the adsorption amount of Fe_3O_4 and Hb in each bilayer is nearly constant, respectively.

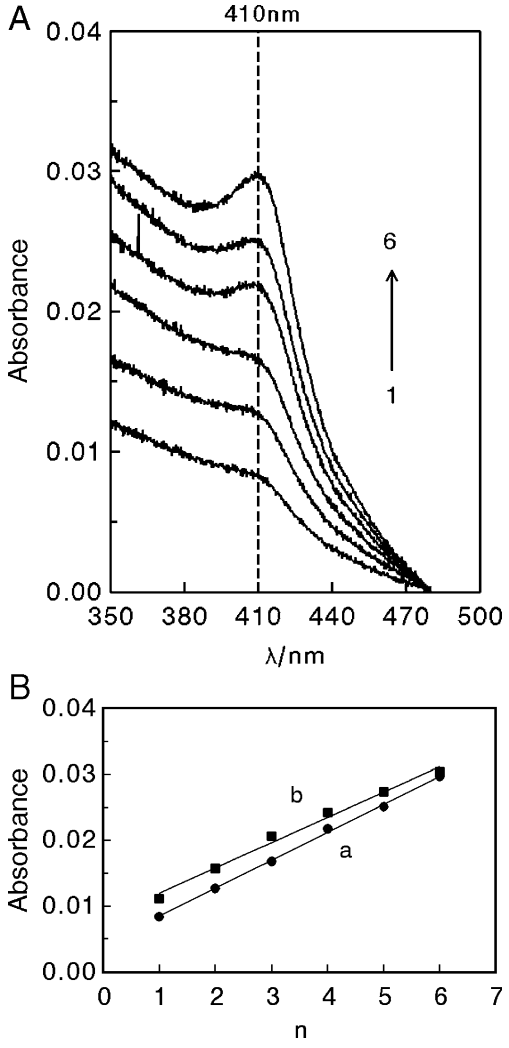

Fig. 2. (A) UV–vis spectra of $\{Fe_3O_4/Hb\}_n$ films on quartz/PEI surface with different number of bilayers (n). (B) Increase of absorbance of $\{Fe_3O_4/Hb\}_n$ films with n (a) at 410 nm and (b) at 360 nm.

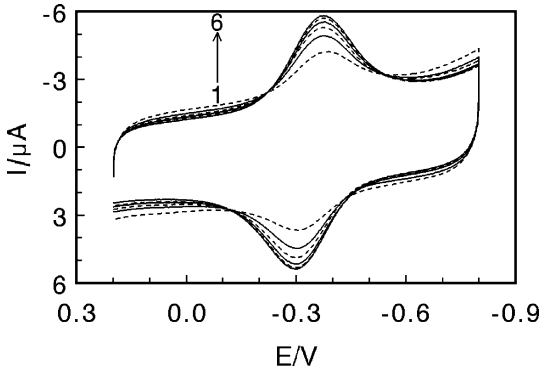

Fig. 3. CVs at 0.2 V s^{-1} in pH 7.0 buffers for $\{Fe_3O_4/Hb\}_n$ films on PG/PEI electrodes with different number of bilayers (n).

From the second adsorption cycle, the frequency increase instead of decrease was observed in the Fe_3O_4 adsorption step. This was probably due to the interaction between Fe_3O_4 and Hb, which led to the removal of some previously adsorbed Hb from the films. Since the mass of desorbed Hb was larger than that of adsorbed Fe_3O_4, the net mass decrease was observed. The similar behavior was also observed in the assembly of other layer-by-layer films [35]. However, the partial removal of Hb did not significantly influence the adsorption of Fe_3O_4 nanoparticles, and the regular growth of the multilayer films kept going.

According to the QCM results of $\{Fe_3O_4/Hb\}_n$ films, the average decrease in frequency caused by each Hb adsorption step was 257±42 Hz. If the density of Hb was assumed to be 1.3 g cm^{-3} [36], this frequency shift for each adsorbed Hb layer would correspond to the nominal thickness of 6.72 nm, which was close to the maximum dimension of Hb molecule ($5.0 \times 5.5 \times 6.5$ nm [37]). This suggests that the Hb adsorption in each assembly cycle results in the formation of monomolecular layer.

Hb has a sensitive Soret absorption band at about 410 nm for its heme groups, and the magnetite absorbs light in the near-UV region [38]. Thus the UV–vis spectroscopy was used to monitor the $\{Fe_3O_4/Hb\}_n$ film growth (Fig. 2A). At both wavelengths of 410 and 360 nm, the absorbance increased linearly with the number of bilayers (Fig. 2B), confirming the assembly of $\{Fe_3O_4/Hb\}_n$ multilayer films and suggesting the uniform growth of the films.

CV was also used to confirm the growth of $\{Fe_3O_4/Hb\}_n$ films by placing the film electrode into pH 7.0 buffers after each assembly cycle (Fig. 3). A pair of chemically reversible reduction–oxidation peaks was observed at about −0.34 V vs SCE, characteristic of HbFe(III)/Fe(II) redox couples. The peaks increased nonlinearly with the number of bilayers (n) up to 6. Hb in the seventh bilayer assembled on the surface of $\{Fe_3O_4/Hb\}_6$ films essentially showed no further increase in CV peak heights, indicating that Hb in the bilayers of $n > 6$ is not electrochemically addressable. Thus, in the following voltammetric studies, $\{Fe_3O_4/Hb\}_6$ films with $n = 6$ were employed.

3.2. CV behavior of $\{Fe_3O_4/Hb\}_6$ films

Both the CV reduction and oxidation peak currents of $\{Fe_3O_4/Hb\}_6$ films increased linearly with scan rates from 0.05 to 2 V s^{-1}. The peaks showed a symmetrical shape and equal heights of reduction and oxidation peaks. All these results were characteristics of the diffusionless, surface-confined voltammetric behavior [39]. In this circumstance, integration of the CV reduction peak gave the charge (Q) value for full reduction of electroactive Hb in the films, and could be used to estimate the surface concentration of electroactive Hb (Γ^*, mol cm^{-2}) [39]. Γ^* increased nonlinearly with n up to 6, and then reached a constant value (Fig. 4a). The Γ^* value of Hb in the first bilayer measured by CV (2.3×10^{-11} mol cm^{-2}) was reasonably close to the Γ value of Hb in each adsorption bilayer estimated by QCM (2.7×10^{-11} mol cm^{-2}). This indicates that the amount of adsorbed Hb in the first bilayer closest to the PG electrode surface is ~100% electroactive. The fraction of electroactive Hb in the following bilayers was thus estimated. Although the total amount of adsorbed Hb in each bilayer was almost the same, the fraction of electroactive Hb decreased drastically with n (Fig. 4b), and Hb could extend to only 6–7 Fe_3O_4/Hb bilayers. This demonstrates that only those Hb molecules in the first few bilayers closest to the electrode surface are electroactive, and the distance between Hb and electrode is crucial for efficient electron exchange. It seems impossible that Hb molecules in the outer layers physically diffuse to the electrode surface in the film phase and then transfer electrons with electrodes. Electron-hopping is therefore the most probable mechanism, in which the efficiency of counterion transport often limits the overall charge transport and the extension of electroactive bilayers in the films [40].

To further confirm the effect of Fe_3O_4 nanoparticles in enhancing the direct electron transfer of Hb, a bare PG electrode was immersed in Hb solution (1 mg mL^{-1}) at pH 5.5 for 120 min, and then transferred into blank buffers at pH 7.0 for CV tests. CV results showed a pair of peaks for adsorbed Hb at the potential of −0.36 V (Fig. 5b), very similar to that of $\{Fe_3O_4/Hb\}_6$ films (Fig. 5c). However, the peak currents of adsorbed Hb at the bare PG electrodes were much smaller than those of $\{Fe_3O_4/Hb\}_6$ films, indicating that much less amounts of Hb are adsorbed directly onto PG surface during the same total immersing time (120 min) in Hb solution, and only a smaller fraction of Hb adsorbed on PG

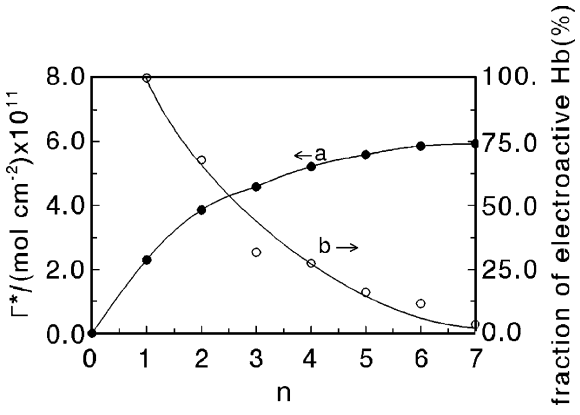

Fig. 4. Influence of the number of bilayers (n) of $\{Fe_3O_4/Hb\}_n$ films on (a) surface concentration of electroactive Hb (Γ^*) and (b) fraction of electroactive Hb. Data are from CV at 0.2 V s^{-1} in pH 7.0 buffers.

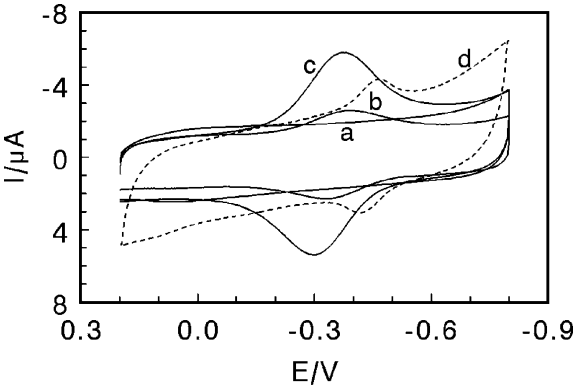

Fig. 5. CVs at 0.2 V s^{-1} in pH 7.0 buffers for (a) Fe_3O_4 monolayer, (b) PG immersed in Hb solution (1 mg mL^{-1}) at pH 5.5 for 120 min, (c) $\{Fe_3O_4/Hb\}_6$ films, and (d) $\{Fe_3O_4/catalase\}_1$ films.

surface is electroactive. In assembly of $\{Fe_3O_4/Hb\}_6$ layer-by-layer films, the adsorption of negatively charged Fe_3O_4 not only has a favorable influence on the adsorption of oppositely charged Hb, leading to more adsorption amounts of Hb, but also provides a favorable microenvironment for Hb to exchange electrons with underlying PG electrodes. The poor CV response of Hb at bare PG electrodes may also be related to the adsorption of macromolecular impurities originally existing in the protein solution, which could block the electron transfer of the proteins [41]. For $\{Fe_3O_4/Hb\}_6$ films, however, the good adsorption selectivity of Fe_3O_4 nanoparticles toward Hb rather than the impurities, combined with the intermediate washing step, may make the assembly procedure act like a purification process. The purity of proteins was reported to be important for the direct electrochemistry of proteins [42]. Another possibility is the better orientation of Hb in $\{Fe_3O_4/Hb\}_6$ films. The orientation of Hb molecules adsorbed on the bare PG surface might be random, while those Hb molecules adsorbed on Fe_3O_4 nanoparticle surface by strong electrostatic interaction may have better order and orientation, which may be beneficial to the electron transfer of Hb with underlying electrodes.

The stability of $\{Fe_3O_4/Hb\}_6$ films were tested by two methods. In the first method, the $\{Fe_3O_4/Hb\}_6$ film electrodes were stored in pH 7.0 buffers all the time, and CVs were measured periodically. Alternatively, $\{Fe_3O_4/Hb\}_6$ films were stored in their dry form in air, and CVs were performed occasionally after returning the dry film electrodes to pH 7.0 buffer solutions. With both methods, the $\{Fe_3O_4/Hb\}_6$ films showed good stability. The reduction peak potentials of the films maintained nearly constant, and the peak currents showed little decrease for at least 20 days.

The CV reduction and oxidation peak positions of $\{Fe_3O_4/Hb\}_6$ films were influenced significantly by the pH of external solution. An increase in pH of the external solutions caused a negative shift in the peak potentials. The formal potentials ($E^{\circ\prime}$), estimated as the average of CV reduction and oxidation peak potentials, had a linear relationship with pH with a slope of -47.5 mV pH^{-1} for $\{Fe_3O_4/Hb\}_6$ films from pH 5.5 to 12. This slope values is reasonably close to the theoretical value of -57.6 at 18 °C for reversible proton-coupled electron transfer with equal number of electrons and protons [43]. Thus, the electrode reaction could be expressed as HemeFe(III)+ $H^+ + e^- \Leftrightarrow$ HemeFe(II).

3.3. Estimation of electrochemical parameters

Square wave voltammetry (SWV), which has better signal-to-noise ratio and resolution than CV [44], was used to estimate the apparent heterogeneous electron transfer rate constant (k_s) and formal potential ($E^{\circ\prime}$) of $\{Fe_3O_4/Hb\}_6$ films. The procedure employed nonlinear regression analysis for SWV forward and reverse curves, using a model that combined the single-species thin-layer SWV model [45] with the $E^{\circ\prime}$ dispersion model, as described in detail previously [46,47]. The analysis of SWV data for $\{Fe_3O_4/Hb\}_6$ films showed accuracy of fits on the $5-E^{\circ\prime}$ dispersion model over a range of pulse amplitudes and frequencies (e. g. Fig. 6). The average k_s value obtained from fitting SWV data at pH 7.0 was 25 s^{-1}, and the average $E^{\circ\prime}$ was -0.355 V vs SCE (Table 1). The $E^{\circ\prime}$ value estimated as a midpoint of CV reduction and oxidation peak potentials for the films is also listed (-0.336 V), which is in good agreement with that obtained by SWV. The electrochemical parameters obtained by the same method for Hb layer-by-layer films with other nanoparticles, as well as cast Hb-Fe_3O_4 films, are also listed in Table 1 for comparison. Although the k_s values for various Hb films are different, they are in the same order of magnitude and relatively large, consistent with the good electrochemical reversibility of Hb in these films shown in cyclic voltammograms. The $E^{\circ\prime}$ value of the heme Fe(III)/Fe(II) couples for Hb in the $\{Fe_3O_4/Hb\}_6$ films is more close to that of cast Hb-Fe_3O_4 films than that for other $\{nanoparticle/Hb\}_6$ films (Table 1), suggesting that the different assembly approach has little influence on $E^{\circ\prime}$ value, and the different film component may have more pronounced effect on the formal potential. Film components may change potentials via interactions with the protein or by their influence on the electrode double layer [4].

The total deposited amount of Hb (Γ, mol cm^{-2}) estimated mainly by QCM, the surface concentration of electroactive Hb

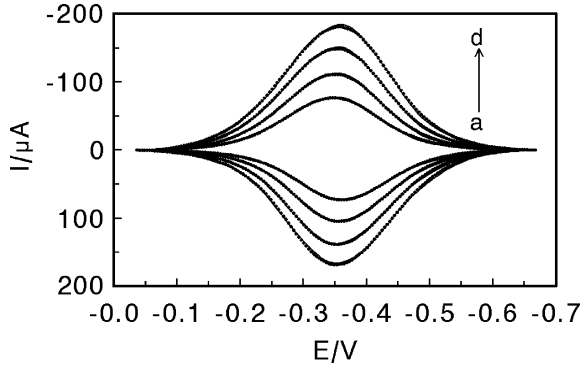

Fig. 6. Square wave forward and reverse current voltammograms for $\{Fe_3O_4/Hb\}_6$ films in pH 7.0 buffers at different frequencies. Points represent experimental background-subtracted SWVs. Solid lines are the best fits by nonlinear regression onto the $5-E^{\circ\prime}$ dispersion model. Pulse height 75 mV, step height 4 mV, and frequencies (Hz): (a) 100, (b) 125, (c) 152, (d) 179.

Table 1
Electrochemical parameters for different Hb films on PG electrodes in pH 7.0 buffers

Films	k_s/s^{-1}[a]	Average $E^{o\prime}$/(V vs SCE)		Total Γ/(mol cm^{-2})	Electroactive Γ^*/ (mol cm^{-2})	Fraction Γ^*/Γ (%)	Reference
		CV	SWV[a]				
$\{Fe_3O_4/Hb\}_6$[b]	25±6	−0.336	−0.355	1.38×10^{-10}	5.86×10^{-11}	42.5	This work
Hb-Fe_3O_4 (cast)	38±4	−0.344	−0.356	6.36×10^{-10}	2.20×10^{-11}	3.34	[28]
$\{clay/Hb\}_6$	42±3	−0.328	−0.346	1.39×10^{-10}	3.69×10^{-11}	26.5	[16]
$\{SiO_2/Hb\}_6$	76±16	−0.328	−0.328	1.58×10^{-10}	6.13×10^{-11}	38.8	[19]
$\{CaCO_3/Hb\}_6$	34±5	−0.351	−0.360	9.60×10^{-11}	3.11×10^{-11}	32.3	[20]

[a] Apparent heterogeneous electron transfer rate constants (k_s) and formal potentials ($E^{o\prime}$) were estimated by SWV with $5-E^{o\prime}$ dispersion model.
[b] k_s and $E^{o\prime}$(SWV) are average values for the analysis of eight SWVs at frequencies of 100–180 Hz, amplitudes of 60–75 mV, and a step height of 4 mV. Γ is from QCM. Γ^* and $E^{o\prime}$(CV) are from CV at 0.2 V s^{-1}.

(Γ^*, mol cm^{-2}) measured by CV, and the fraction of electroactive Hb in the films (Γ^*/Γ) for various {nanoparticle/Hb}$_6$ films with the same 6 bilayers and cast Hb-Fe_3O_4 films are also listed in Table 1. The layer-by-layer $\{Fe_3O_4/Hb\}_6$ films exhibited more than 10 times larger fraction of Γ^*/Γ (42.5%) than cast Hb-Fe_3O_4 films (3.34%), demonstrating that the layer-by-layer films can utilize the protein more efficiently than the cast films in protein electrochemistry. On the other hand, while $\{Fe_3O_4/Hb\}_6$ films showed a larger value of Γ^*/Γ compared with that of other {nanoparticle/Hb}$_6$ layer-by-layer films, all of them were at the same level ranging from 26% to 43%. Different {nanoparticle/Hb}$_6$ films exhibited the similar Γ^*/Γ ratio independent of the type of nanoparticles, indicating the general or common properties of inorganic nanoparticles in enhancing electron exchange of Hb with underlying electrodes.

3.4. Conformational studies

The positions of Soret band of Hb can provide some information about the protein conformation, especially in the heme region [48,49], and UV–vis spectroscopy was used here to examine the possible denaturation of Hb in $\{Fe_3O_4/Hb\}_6$ films (Fig. 7). The results demonstrated that the Soret band of dry $\{Fe_3O_4/Hb\}_6$ films assembled on quartz slides was located at 410 nm, while dry Hb films showed the Soret band at 412 nm. The much closed Soret band position of the two films suggests that Hb in dry $\{Fe_3O_4/Hb\}_6$ films retains its near native conformation, while the 2 nm difference in Soret band position may be attributed to the different microenvironment where Hb resides. When the $\{Fe_3O_4/Hb\}_6$ films were immersed into buffers at pH between 5.5 and 11.0, the Soret band appeared at 410 nm, same as for dry $\{Fe_3O_4/Hb\}_6$ films, indicating that Hb in the films essentially retains its native state at medium pH. When pH was changed toward more acidic direction, the Soret band showed a blue shift. For example, at pH 3.0, the Soret band shifted to 400 nm and became broader, suggesting that Hb in $\{Fe_3O_4/Hb\}_6$ films may denature to some extent in this more acidic environment.

To further investigate the possibility of release of the heme groups from Hb polypeptide matrix in the assembly of $\{Fe_3O_4/Hb\}_n$ films, CVs of $\{Fe_3O_4/catalase\}_1$ films assembled on PG electrodes were conducted (Fig. 5d). Catalase is also a kind of heme proteins with MW of 240,000 and four similar subunits, each of which contains a heme group. The $\{Fe_3O_4/catalase\}_n$ films were prepared in the same way as the corresponding Hb films on PG, and the peak current increase was not observed even after $n=2$. While the CV response of $\{Fe_3O_4/catalase\}_1$ films was small, the direct and nearly reversible electrochemistry of catalase was clearly observed, and the peak potentials at around −0.44 V was believed to be attributed to catalase heme Fe(III)/Fe(II) redox couples [50]. The midpoint peak potential of $\{Fe_3O_4/catalase\}_1$ films was about 0.1 V more negative than that of $\{Fe_3O_4/Hb\}_6$ films, indicating that the different proteins with the same prosthetic group or redox center may not have the same redox formal potential in the same microenvironment, as observed also in the previous work [51,52]. If the proteins in $\{Fe_3O_4/protein\}_n$ films were denatured and most of the heme groups were split out of the polypeptide matrix, the CV peak potentials of $\{Fe_3O_4/Hb\}_6$ and $\{Fe_3O_4/catalase\}_1$ films should have been the same. We thus speculate that the heme groups of

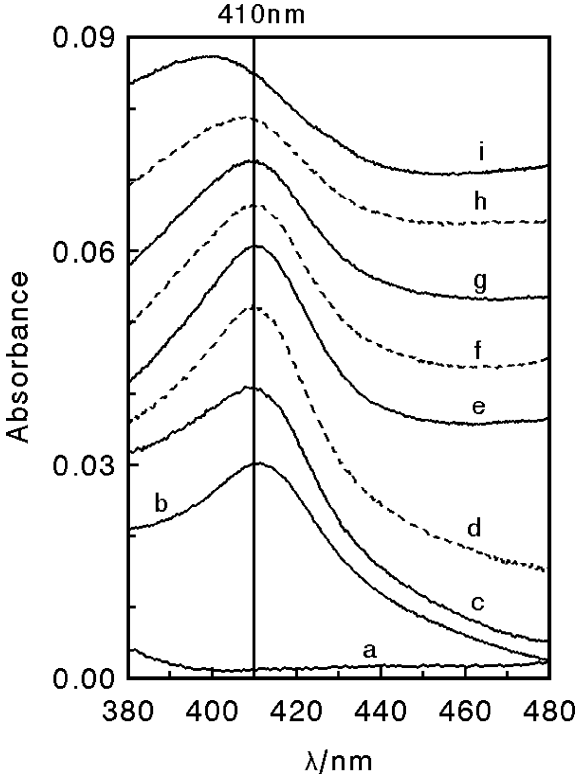

Fig. 7. UV–vis spectra for (a) dry Fe_3O_4 films, (b) dry Hb films, (c) dry $\{Fe_3O_4/Hb\}_6$ films, and $\{Fe_3O_4/Hb\}_6$ films in buffers at different pH: (d) pH 7.0; (e) pH 5.5; (f) pH 9.0; (g) pH 11.0; (h) pH 4.0; (i) pH 3.0.

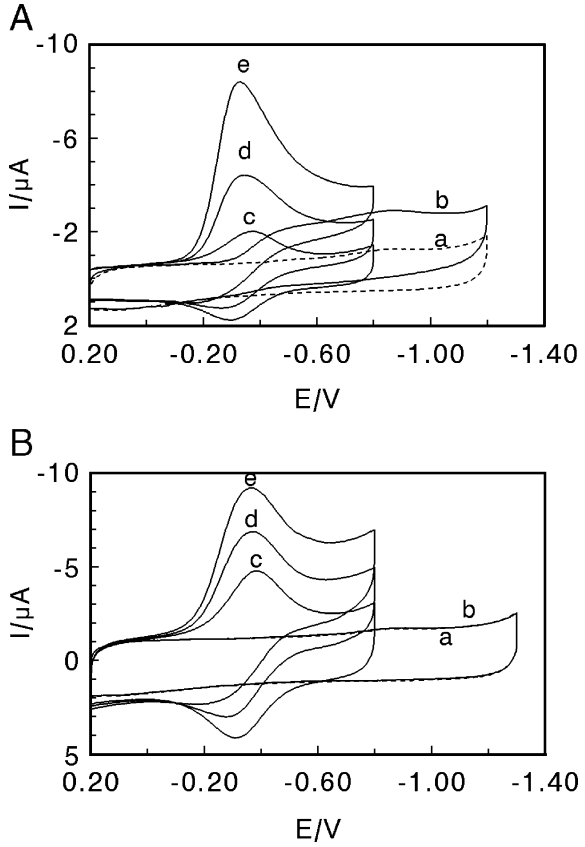

Fig. 8. (A) CVs at 0.2 V s^{-1} in 10 mL of pH 7.0 buffers for (a) Fe_3O_4 monolayer, (b) Fe_3O_4 monolayer after 10 mL of air was injected in sealed cell, (c) $\{Fe_3O_4/Hb\}_6$ films, (d) $\{Fe_3O_4/Hb\}_6$ films with 5 mL of air, and (e) $\{Fe_3O_4/Hb\}_6$ films with 10 mL of air. (B) CVs at 0.2 V s^{-1} in pH 7.0 buffers for (a) Fe_3O_4 monolayer, (b) Fe_3O_4 monolayer in buffers containing 0.028 mM H_2O_2, (c) $\{Fe_3O_4/Hb\}_6$ films, (d) $\{Fe_3O_4/Hb\}_6$ films with 0.012 mM H_2O_2, and (e) $\{Fe_3O_4/Hb\}_6$ films with 0.028 mM H_2O_2.

Hb are kept inside the polypeptide pockets and not released from the protein matrix in $\{Fe_3O_4/Hb\}_n$ films.

3.5. Electrocatalytic activity

Electrocatalytic reduction of oxygen by $\{Fe_3O_4/Hb\}_6$ films was examined by CV. When a certain amount of air was passed through a pH 7.0 buffer by a syringe, an obvious increase in reduction peak at about −0.36 V was observed for $\{Fe_3O_4/Hb\}_6$ films, accompanied by the disappearance of the oxidation peak of HbFe(II), suggesting that HbFe(II) had reacted with oxygen (Fig. 8A). The reduction peak current increased with the amount of oxygen in solution. For the Fe_3O_4 monolayer adsorbed on PG/PEI surface, a broad peak for direct reduction of oxygen was observed at about −0.80 V, more negative than the catalytic peak potential. Thus, the overpotential required for reduction of O_2 was lowered by about 0.34 V by $\{Fe_3O_4/Hb\}_6$ films. Catalytic efficiency, expressed as the ratio of reduction peak current in the presence (I_c) and absence of oxygen (I_d), I_c/I_d, decreased with increase of scan rate, also characteristic of electrochemical catalytic reduction of oxygen by Hb in $\{Fe_3O_4/Hb\}_6$ films [53].

Electrochemical catalytic reaction of hydrogen peroxide was also observed at $\{Fe_3O_4/Hb\}_6$ film electrodes (Fig. 8B). When H_2O_2 was added to a pH 7.0 buffer, an increase in the reduction peak at about −0.4 V was observed with the decrease of the oxidation peak for HbFe(II). The reduction peak current increased with the concentration of H_2O_2 in solution. However, no direct reduction peak was observed at Fe_3O_4 monolayer electrodes when H_2O_2 was present.

The catalytic reduction of trichloroacetic acid (TCA) at the $\{Fe_3O_4/Hb\}_6$ film electrodes was also tested by CV. When TCA was added to the buffer, the HbFe(III) reduction peak of $\{Fe_3O_4/Hb\}_6$ films increased in height (Fig. 9A), accompanied by the decrease of HbFe(II) oxidation peak. The reduction peak current increased with TCA concentration. All these results are characteristic of electrochemical catalysis, in which HbFe(II) produced in electrode reaction was chemically oxidized by TCA and returned to HbFe(III) again, forming the catalytic cycle. Compared with the direct reduction of TCA on Fe_3O_4 monolayer films without Hb, $\{Fe_3O_4/Hb\}_6$ films lowered the reduction overpotential of TCA by at least 0.7 V, indicating a large decrease in activation energy for TCA reduction.

The $\{Fe_3O_4/Hb\}_6$ film electrodes were also used to catalyze reduction of nitrite. A new reduction peak appeared at about −0.75 V when NO_2^- was added in a pH 5.5 buffer (Fig. 9B), and the peak increased with a further addition of NO_2^-. Direct

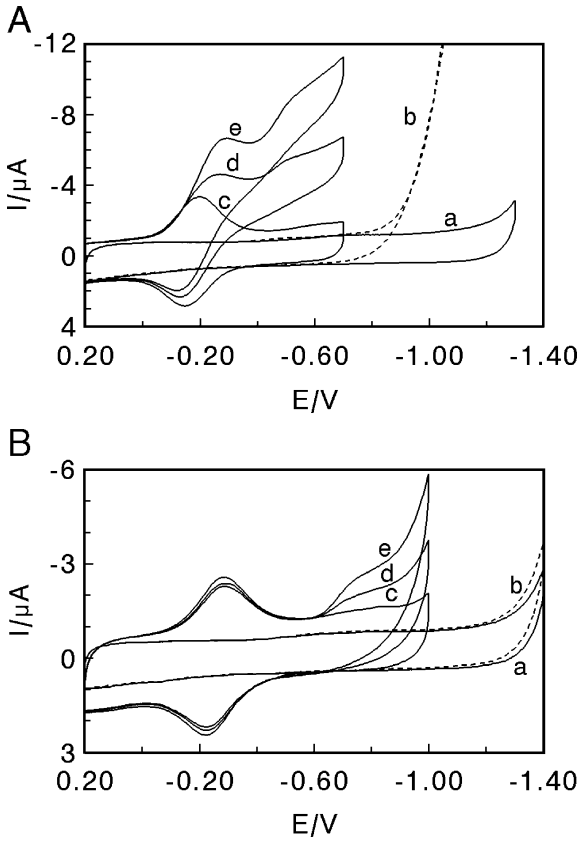

Fig. 9. (A) CVs at 0.1 V s^{-1} at pH 3.0 for (a) Fe_3O_4 monolayer, (b) Fe_3O_4 monolayer in buffers containing 1.6 mM TCA, (c) $\{Fe_3O_4/Hb\}_6$ films, (d) $\{Fe_3O_4/Hb\}_6$ films with 1.6 mM TCA, and (e) $\{Fe_3O_4/Hb\}_6$ films with 3.9 mM TCA. (B) CVs at 0.1 V s^{-1} at pH 5.5 for (a) Fe_3O_4 monolayer, (b) Fe_3O_4 monolayer in buffers containing 1.98 mM NO_2^-, (c) $\{Fe_3O_4/Hb\}_6$ films, (d) $\{Fe_3O_4/Hb\}_6$ films with 0.80 mM NO_2^-, and (e) $\{Fe_3O_4/Hb\}_6$ films with 1.98 mM NO_2^-.

reduction of NO_2^- on Fe_3O_4 monolayer films containing no Hb was found at the potential more negative than −1.3 V. Thus, $\{Fe_3O_4/Hb\}_6$ films decreased the reduction overpotential of NO_2^- by at least 0.55 V. The species that catalytically reduced at the film electrodes is most probably NO since nitrite would become NO in acid media, while the direct evidence for this is absent by now.

The good biocatalytic activity of Hb incorporated in multilayered $\{Fe_3O_4/Hb\}_6$ films toward various substrates may establish a foundation for fabricating the new kind of biosensors or bioreactors without using chemical mediators.

4. Conclusion

Under the optimized conditions, layer-by-layer films of hemoglobin with magnetic Fe_3O_4 nanoparticles were successfully assembled on various solid surfaces mainly by electrostatic interaction between them. The direct electron transfer of Hb with underlying PG electrodes in $\{Fe_3O_4/Hb\}_6$ films involving Hb heme Fe(III)/Fe(II) redox couples was much faster than that for Hb in solution on bare PG electrodes. This is a new example of layer-by-layer self-assembly of heme proteins with inorganic nanoparticles, which exhibits the direct electrochemistry of proteins. Hb essentially retained its native conformation in the $\{Fe_3O_4/Hb\}_6$ films, and the heme groups inside the Hb polypeptide matrix did not split out of the pockets . Good electrocatalytic reactivity of Hb in $\{Fe_3O_4/Hb\}_n$ films for the reduction of various substrates with biological or environmental significance suggests that the films have a promising potential in constructing the third-generation electrochemical biosensor based on the direct electrochemistry of enzymes.

Acknowledgments

The financial support from the National Natural Science Foundation of China (20275006, 20475008) is acknowledged.

References

[1] J.F. Rusling, Z. Zhang, in: R.W. Nalwa (Ed.), Handbook of Surfaces and Interfaces of Materials, vol. 5, Academic Press, New York, 2001, pp. 33–71.
[2] N. Hu, Direct electrochemistry of redox proteins or enzymes at various film electrodes and their possible applications in monitoring some pollutants, Pure Appl. Chem. 73 (2001) 1979–1991.
[3] F.A. Armstrong, G.S. Wilson, Recent developments in Faradaic bioelectrochemistry, Electrochim. Acta 45 (2000) 2623–2645.
[4] J.F. Rusling, Enzyme bioelectrochemistry in cast biomembrane-like films, Acc. Chem. Res. 31 (1998) 363–369.
[5] G. Decher, Fuzzy nanoassemblies: toward layered polymeric multicomposites, Science 277 (1997) 1232–1237.
[6] Y. Lvov, in: Y. Lvov, H. Mohwald (Eds.), Protein Architecture: Interfacing Molecular Assemblies and Immobilization Biotechnology, Marcel Dekker, New York, 2000, pp. 125–166.
[7] Y. Lvov, in: R.W. Nalwa (Ed.), Handbook of Surfaces and Interfaces of Materials, vol. 3, Academic Press, New York, 2001, pp. 170–189.
[8] Y. Lvov, Z. Lu, J.B. Schenkman, X. Zu, J.F. Rusling, Direct electrochemistry of myoglobin and cytochrome P450cam in alternate layer-by-layer films with DNA and other polyions, J. Am. Chem. Soc. 120 (1998) 4073–4080.
[9] J.B. Schenkman, I. Jansson, Y. Lvov, J.F. Rusling, S. Boussaad, N.J. Tao, Charge-dependent sidedness of cytochrome P450 forms studied by quartz crystal microbalance and atomic force microscopy, Arch. Biochem. Biophys. 385 (2001) 78–87.
[10] H. Ma, N. Hu, J.F. Rusling, Electroactive myoglobin films grown layer-by-layer with poly(styrenesulfonate) on pyrolytic graphite electrodes, Langmuir 16 (2000) 4969–4975.
[11] P. He, N. Hu, G. Zhou, Assembly of electroactive layer-by-layer films of hemoglobin and polycationic poly(diallyldimethyl ammonium), Biomacromolecules 3 (2002) 139–146.
[12] L. Wang, N. Hu, Direct electrochemistry of hemoglobin in layer-by-layer films with poly(vinyl sulfonate) grown on pyrolytic graphite electrodes, Bioelectrochemistry 53 (2001) 205–212.
[13] N. Kimizuka, M. Tanaka, T. Kunitake, Spatially controlled synthesis of protein/inorganic nano-assembly: alternate molecular layers of cyt c and TiO_2 nanoparticles, Chem. Lett. (1999) 1333–1334.
[14] F. Patosky, T. Gabriel, I. Willner, Controlled electrocatalysis by microperoxidase-11 and Au-nanoparticle superstructures on conductive supports, J. Electroanal. Chem. 479 (1999) 69–73.
[15] Y. Lvov, B. Munge, O. Giraldo, I. Ichinose, S.L. Suib, J.F. Rusling, Films of manganese oxide nanoparticles with polycations or myoglobin from alternate-layer adsorption, Langmuir 16 (2000) 8850–8857.
[16] Y. Zhou, Z. Li, N. Hu, Y. Zeng, J.F. Rusling, Layer-by-layer assembly of ultrathin films of hemoglobin and clay nanoparticles with electrochemical and catalytic activity, Langmuir 18 (2002) 8573–8579.
[17] Z. Li, N. Hu, Direct electrochemistry of heme proteins in their layer-by-layer films with clay nanoparticles, J. Electroanal. Chem. 558 (2003) 155–165.
[18] P. He, N. Hu, J.F. Rusling, Driving forces for layer-by-layer self-assembly of films of SiO_2 nanoparticles and heme proteins, Langmuir 20 (2004) 722–729.
[19] P. He, N. Hu, Electrocatalytic properties of heme proteins in layer-by-layer films assembled with SiO_2 nanoparticles, Electroanalysis 16 (2004) 1122–1131.
[20] H. Liu, N. Hu, Comparative bioelectrochemical study of core-shell nanocluster films with ordinary layer-by-layer films containing heme proteins and $CaCO_3$ nanoparticles, J. Phys. Chem., B 109 (2005) 10464–10473.
[21] I. Safarik, M. Safarikova, Magnetic nanoparticles and biosciences, Monatsh. Chem. 133 (2002) 737–759.
[22] I. Willner, B. Willner, Functional nanoparticle architectures for sensoric, optoelectronic, and bioelectronic applications, Pure Appl. Chem. 74 (2002) 1773–1783.
[23] P.A. Dresco, V.S. Zaitsev, R.J. Gambino, B. Chu, Preparation and properties of magnetite and polymer magnetite nanoparticles, Langmuir 15 (1999) 1945–1951.
[24] R.V. Mehta, R.V. Upadhyay, S.W. Charles, C.N. Ramchand, Direct binding of protein to magnetic particles, Biotechnol. Tech. 11 (1997) 493–496.
[25] M. Koneracka, P. Kopcansky, M. Antalik, M. Timko, C.N. Ramchand, D. Lobo, R.V. Mehta, R.V. Upadhyay, Immobilization of proteins and enzymes to fine magnetic particles, J. Magn. Magn. Mater. 201 (1999) 427–430.
[26] D.-H. Chen, M.-H. Liao, Preparation and characterization of YADH-bound magnetic nanoparticles, J. Mol. Catal., B Enzym. 16 (2002) 283–291.
[27] M.T. Reetz, A. Zonta, V. Vijayakrishnan, K. Schimossek, Entrapment of lipases in hydrophobic magnetite-containing sol–gel materials: magnetic separation of heterogeneous biocatalysts, J. Mol. Catal., A Chem. 134 (1998) 251–258.
[28] D. Cao, P. He, N. Hu, Electrochemical biosensors utilising electron transfer in heme proteins immobilised on Fe_3O_4 nanoparticles, Analyst 128 (2003) 1268–1274.
[29] C. Lu, C. Luo, W. Cao, Self-assembly of a covalently attached magnetic film from diazoresin and Fe_3O_4 nanoparticles, J. Mater. Chem. 13 (2003) 382–384.
[30] Y. Liu, A. Wang, R.O. Claus, Layer-by-layer electrostatic self-assembly of nanoscale Fe_3O_4 particles and polyimide precursor on silicon and silica surfaces, Appl. Phys. Lett. 71 (1997) 2265–2267.

[31] A.A. Mamedov, N.A. Kotov, Free-standing layer-by-layer assembled films of magnetite nanoparticles, Langmuir 16 (2000) 5530–5533.
[32] G.D. Mendenhall, Y. Geng, J. Hwang, Optimization of long-term stability of magnetic fluids from magnetite and synthetic polyelectrolytes, J. Colloid Interface Sci. 184 (1996) 519–526.
[33] J.B. Matthew, G.I.H. Hanania, F.R.N. Gurd, Electrostatic effects in hemoglobin-hydrogen-ion equilibria in human deoxyhemoglobin and oxyhemoglobin-A, Biochemistry 18 (1979) 1919–1928.
[34] G. Sauerbrey, Verwendung von schwingquarzen zur wagung dunner schichten und zur mikrowagung, Z. Phys. 155 (1959) 206–214.
[35] A.J. Khopade, F. Caruso, Investigation of the factors influencing the formation of dendrimer/polyanion multilayer films, Langmuir 18 (2002) 7669–7676.
[36] T.E. Creighton (Ed.), Protein Structure, A Practical Approach, IRL Press, New York, 1990, p. 43.
[37] M.F. Perutz, H. Muirhead, J. Cox, L. Goaman, L. Mathews, E. Mcgandy, L. Webb, 3-Dimensional Fourier synthesis of horse oxyhaemoglobin at 2.8 Å resolution: I. X-ray analysis, Nature 219 (1968) 29.
[38] A. Mamedov, J. Ostrander, F. Aliev, N.A. Kotov, Stratified assemblies of magnetite nanoparticles and montmorillonite prepared by the layer-by-layer assembly, Langmuir 16 (2000) 3941–3949.
[39] R.W. Murray, in: A.J. Bard (Ed.), Electroanalytical Chemistry, vol. 13, Marcel Dekker, New York, 1986, pp. 191–368.
[40] M. Majda, in: R.W. Murray (Ed.), Molecular Design of Electrode Surfaces, Wiley, New York, 1992, pp. 159–206.
[41] A.-E.F. Nassar, W.S. Willis, J.F. Rusling, Electron transfer from electrodes to myoglobin: facilitated in surfactant films and blocked by adsorbed biomacromolecules, Anal. Chem. 67 (1995) 2386–2392.
[42] I. Taniguchi, K. Watanabe, M. Tominaga, F.M. Hawkridge, Direct electron-transfer of horse heart myoglobin at an indium oxide electrode, J. Electroanal. Chem. 333 (1992) 331.
[43] A.M. Bond, Modern Polarographic Methods in Analytical Chemistry, Dekker, New York, 1980.
[44] J.G. Osteryoung, J.J. O'Dea, in: A.J. Bard (Ed.), Electroanalytical Chemistry, vol. 14, Marcel Dekker, New York, 1986, pp. 209–325.
[45] J.J. O'Dea, J.G. Osteryoung, Characterization of quasi-reversible surface processes by square-wave voltammetry, Anal. Chem. 65 (1993) 3090–3097.
[46] Z. Zhang, J.F. Rusling, Electron transfer between myoglobin and electrodes in thin films of phosphatidylcholines and dehexadecylphosphate, Biophys. Chem. 63 (1997) 133–146.
[47] A.-E.F. Nassar, Z. Zhang, N. Hu, J.F. Rusling, T.F. Kumosinski, Proton-coupled electron transfer from electrodes to myoglobin in ordered biomembrane-like films, J. Phys. Chem., B 101 (1997) 2224–2231.
[48] H. Theorell, A. Ehrenberg, Spectrophotometric, magnetic, and titrimetric studies on the heme-linked groups in myoglobin, Acta Chem. Scand. 5 (1951) 823–848.
[49] P. George, G.I.H. Hanania, Spectrophotometric study of ionizations in methemoglobin, Biochem. J. 55 (1953) 236–243.
[50] Z. Zhang, S. Chouchane, R.S. Magliozzo, J.F. Rusling, Direct voltammetry and catalysis with mycobacterium tuberculosis catalase-peroxidase, peroxidases, and catalase in lipid films, Anal. Chem. 74 (2002) 163–170.
[51] L. Shen, N. Hu, Heme-protein films with polyamidoamine dendrimer: direct electrochemistry and electrocatalysis, Biochim. Biophys. Acta, Bioenerg. 1608 (2004) 23–33.
[52] H. Huang, N. Hu, Y. Zeng, G. Zhou, Electrochemistry and electrocatalysis with heme proteins in chitosan biopolymer films, Anal. Biochem. 308 (2002) 141–151.
[53] C.P. Andrieux, C. Blocman, J.-M. Dumas-Bouchiant, F. M'Halla, J.M. Saveant, Homogeneous redox catalysis of electrochemical reactions: Part V. Cyclic voltammetry, J. Electroanal. Chem. 113 (1980) 19–40.